Available online at www.sciencedirect.com
SCIENCE DIRECT®

Journal of the European Ceramic Society 24 (2004) 775–783

www.elsevier.com/locate/jeurceramsoc

Effect of polarization on fracture toughness of $BaTiO_3/Al_2O_3$ composites

Sirirat Rattanachan, Yukio Miyashita, Yoshiharu Mutoh*

Department of Mechanical Engineering, Nagaoka University of Technology, 1603-1 Kamitomioka, Nagaoka-shi 940-2188, Japan

Received 11 September 2002; received in revised form 15 April 2003; accepted 27 April 2003

Abstract

In this study, Al_2O_3 based composites dispersed with $BaTiO_3$ particles were fabricated by a conventional sintering process. The relative density and microstructure (grain size, phase) of composites were studied. The relative density of $BaTiO_3/Al_2O_3$ composites decreased with increasing $BaTiO_3$ content, and there were reaction phases between Al_2O_3 matrix and dispersed $BaTiO_3$ particles. The Indentation Fracture Method was used to evaluate the fracture toughness of the present composites before and after polarization. It was verified that an applied electric field induced distinct anisotropy in fracture toughness of $BaTiO_3/Al_2O_3$ composites between parallel and perpendicular directions to the poling direction. The fracture toughness was improved with addition of $BaTiO_3$ particles to Al_2O_3 matrix. The toughening mechanisms of $BaTiO_3/Al_2O_3$ composites have been also discussed.

Keywords: Al_2O_3; $BaTiO_3$; Composites; Ferroelectric properties; Fracture toughness; Piezoelectric properties; Polarization

1. Introduction

Since ceramics is brittle in nature, a variety of approaches to enhance their fracture resistance have been reported. Recently, novel composite materials that exhibit excellent functional as well as mechanical properties have been developed for advanced engineering applications. Among them, ceramic matrix composites with the ferroelectric/piezoelectric secondary dispersoids have been proposed. The electromechanical properties of ferroelectric/piezoelectric phases induced interesting functions into the composites. By utilizing electromechanical properties of the ferroelectric material, it is possible to detect a crack propagation.[1] When an electric field is applied to the ferroelectric materials, anisotropic internal stresses induced can increase or decrease fracture toughness, which depending on the poling direction.[2] Ferroelectric particles dispersed in the ceramic matrix composite are expected to exhibit such smart functions that are capable of predicting the fracture, which electric signal can be detected during crack propagation, and controlling the crack. In the past few years, Niihara and his colleagues have proposed a ferroelectric nanocomposite with high strength and toughness such as PZT/Pt,[3] $BaTiO_3/MgO$[4] and $BaTiO_3/SiC$[5] and many researchers have extensively investigated its excellent mechanical properties and also in such electrical properties as dielectric constant, the Curie temperature, and so on. Various compositions such as $BaTiO_3/Al_2O_3$,[6] $BaTiO_3$/3Y–TZP,[7] $Nd_2Ti_2O_7/Al_2O_3$,[8] $Sr_2Nb_2O_7$/3Y–TZP[9] and $BaTiO_3/ZrO_2$[10] composites have been studied. High fracture toughness has been recently achieved for a $BaTiO_3$ toughened Al_2O_3 system,[6] where the fracture toughness reached 5.1 MPa $m^{1/2}$ for a composition of 5 mol% $BaTiO_3$ in Al_2O_3 matrix composites, while that of a monolithic Al_2O_3 is around 4 MPa $m^{1/2}$. In this work, only unpoled samples were used and effect of poling was not clear.

The Vickers indentation technique under a static electric field has been widely used for investigating fracture toughness of poled ferroelectric ceramics. Schneider and Heyer[11] used the Vickers indention method to investigate the crack growth behavior of ferroelectric barium titanate ceramics under the influence of the electric fields. The result verified that an applied electric field induced distinct anisotropy between crack

* Corresponding author. Tel.: +81-258-47-9735; fax: +81-258-47-9770.

E-mail address: mutoh@mech.nagaokaut.ac.jp (Y. Mutoh).

0955-2219/03/$ - see front matter
doi:10.1016/S0955-2219(03)00319-4

growth parallel and perpendicular to the poling direction, which was mainly interpreted as an anisotropy in fracture toughness. Stress-induced ferroelastic domain switching is used to explain the observed anisotropy of crack length and fracture toughness.

The fracture toughness of piezoelectric ceramics is affected by many factors, including temperature, microstructure, chemical composition, poling, and external electrical and mechanical loading. Several mechanisms have been suggested for the toughening of the ferroelectric phase, including microcracking and crack/domain wall (twin) interaction,[12–14] and domain switching (the c–axis becomes perpendicular to the crack surface) in the stress field near a crack tip.[13–16]

In the present work, Al_2O_3 based composites with 3 and 5 mol% $BaTiO_3$ secondary phases have been fabricated by the pressureless sintering method. Although composition of the present composites are the same as Ref. 6, the starting powders were different and the present composites were fabricated by using cold isostatic pressing to obtain higher relative density. Microstructures of the composites were investigated in terms of $BaTiO_3$ content and sintering temperature. To investigate fracture toughness improvement of the composites due to the piezoelectric secondary phase and energy dissipation by piezoelectric effect, Vickers indentation method was employed to measure the fracture toughness before and after polarization. The toughening mechanisms of $BaTiO_3/Al_2O_3$ composites have been discussed.

2. Experimental procedure

2.1. Material preparation

Commercial barium titanate (BT-05, Sakai chemical industrial Co. Ltd.) with an average particle size of 0.5 μm and high purity alumina (Sumitomo Sekitan Kougyo, KK) powders with an average particle size of 0.2 μm were used as the starting materials. Al_2O_3 powders with 3 and 5 mol% $BaTiO_3$ powders were mixed by ball milling with alumina balls in ethanol for 24 h. The wet slurry was then dried by a rotary evaporator. Dried powders were milled again and sieved through 150 μm mesh screen.

The mixed granules with PVA as a binder were formed into rectangular bars by uniaxially pressing and then pressed by cold isostatic pressing (CIP) at 200 MPa. Then, the compacts were fired in furnace at temperatures of 1400 and 1450 °C for 2 h in air with a heating rate of 10 °C/min. Dimensions of the bar were 15 mm in width and 80 mm length. The monolithic alumina was also prepared by the same sintering method, while its sintering temperature was 1500 °C.

2.2. Material characterization

The bulk density was determined by Archimedes' method in water. The X-ray diffraction pattern was taken using X-ray diffractometer (Shimadzu XRD 6100) with nickel-filtered CuK_α radiation. The specimen surface was polished and then thermal etched at 1350 °C for 10 min. The average grain sizes and microstructure of the specimens were evaluated on the polished and etched surfaces using a scanning electron microscope.

2.3. Fracture toughness testing

The test specimens (3×4×35 mm) were directly cut from the sintered samples using a diamond wheel. Dimensions and shape of the specimen are shown in Fig. 1. Polarization of the composite specimens was made as follows: The 3×35 mm specimen surfaces were polished using 800 mesh SiC paper and then applied silver paste as electrode and dried in air oven at 120 °C for 10 min. The poling was carried out under the electric field of 3.75 kV/mm at 120 °C for 10 min. The electric field of 3.75 kV/mm for poling of the composites is significantly high compared that of monolithic $BaTiO_3$ (0.5–0.6 kV/mm) due to much smaller relative permittivity of Al_2O_3 phase. These values of electric field for poling corresponds to the maximum point, over which the electric current suddenly increases. The surface for indentation was polished using successively finer diamond pastes from 1 μm down to 0.2 μm. The indentation surface was parallel to the poling direction.

The Vickers indentation test was conducted at room temperature using a load of 98 N for a constant duration of 15 s. In order to investigate the effect of poling direction on fracture toughness, two diagonal directions of the indenter, that is (a) 45°-direction and (b) 90°-direction, were applied, as schematically shown in Fig. 2. After unloading, the crack lengths were measured immediately in the two orthogonal radial directions (see Fig. 2), respectively. $c_\perp$ and $c_\parallel$ were denoted to the crack lengths perpendicular and parallel to the poling direction, respectively. At least 20 measurements of the crack length were taken for each data point, and the average and standard deviation were calculated.

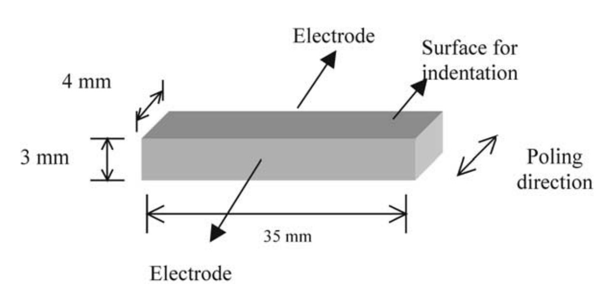

Fig. 1. Specimen dimensions, electrode/indentation surfaces and poling direction.

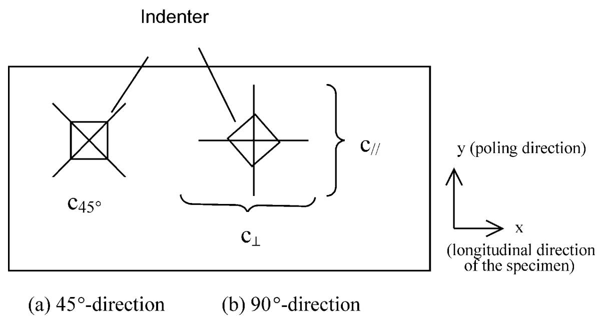

Fig. 2. Relative direction between specimen and indenter on the indenting surface.

Fracture toughness was calculated using the equation proposed by Niihara et al.[17] The indentation crack paths were observed in detail using a scanning electron microscope (SEM).

2.4. Residual stress measurement

In order to investigate the residual stress of Al_2O_3 matrix induced by poling, the X-ray stress measurement (Shimadzu XRD 6100) was conducted. The conditions of X-ray stress measurement are shown in Table 1. The diffraction from Al_2O_3 (146) plane by Cu-K_α was recorded with the side-inclination (φ angle) method. The X-ray stress constant (S) for determining stress by the $\sin^2\varphi$ method was calculated from various applied stresses (σ_A) of the alumina sample sintered at 1500 °C:

$$S = -\frac{E}{2(1+\upsilon)}\cot\theta_0 \quad (1)$$

where θ_0 is the diffraction angle for stress-free materials.

$$\frac{2(1+\upsilon)}{E} = -\cot\theta_0\left(\frac{\partial M}{\partial\sigma_A}\right) \quad (2)$$

The stress was evaluated from the slope M of the $\sin^2\varphi$ diagram as.[18]

$$\sigma_x = S.M \quad (3)$$

Since the residual stresses might be unavoidably introduced on the surfaces during grinding and machining, all specimens were annealed to eliminate the residual stress due to polishing and machining. The residual stresses corresponding to perpendicular and parallel to the poling direction are denoted by $\sigma_\perp$ and $\sigma_\parallel$, respectively.

Table 1
Conditions for X-ray stress measurement

Method	Parallel beam method
Characteristic X-ray	CuK_α
Diffraction plane	Al_2O_3 (146)
Diffraction angle (°)	136.30
Filter	Ni
Tube voltage (kV)	40
Tube current (mA)	30
Scanning speed (°/min)	2.0
Preset time (s)	4.0
Inclination planes (°)	0, 10, 20, 30, 35, 40 and 45

3. Results and discussion

3.1. Characterization of $BaTiO_3/Al_2O_3$ composites

From Table 2, $BaTiO_3/Al_2O_3$ composites indicated lower relative density compared to monolithic Al_2O_3. Their relative density and hardness decreased with the increasing $BaTiO_3$ content. X-ray diffraction analysis of each composition was carried out to evaluate the relative intensity of intermediate phases, i.e. $BaAl_6TiO_{12}$ and $BaAl_{13.2}O_{20.8}$, to the Al_2O_3 phase. Since the XRD peaks of $BaTiO_3$ almost coincide with those of $BaAl_6TiO_{12}$ peaks, the quantitative evaluation of $BaTiO_3$ phase in sintered specimens was difficult. The results are shown in Table 2.

Image analysis of Al_2O_3 matrix composites with 3 and 5 mol% $BaTiO_3$ contents was conducted to evaluate the microstructure and average grain sizes. Average grain sizes of the composites evaluated were listed in Table 2. Fig. 3 shows the typical microstructures of the thermal etched surfaces of 3 and 5 mol% $BaTiO_3/Al_2O_3$ composites. The $BaTiO_3$ and intermediate phases, the white and gray regions, respectively, as shown in Fig. 3, are not uniformly dispersed in the matrix. The shapes of the dispersed phases were also irregular. With increasing the $BaTiO_3$ and sintering temperature, the reaction between $BaTiO_3$ and Al_2O_3 increased and consequently the amount of intermediate phases increased. However, the average matrix grain sizes decreased compared to the monolithic Al_2O_3. The intermediate phases (i.e. $BaAl_6TiO_{12}$ and $BaAl_{13.2}O_{20.8}$) were observed, as gray region in the micrograph, clearly around $BaTiO_3$ phase (white region). It can be indicated that the reaction between $BaTiO_3$ and Al_2O_3 occurs at the surface of $BaTiO_3$ and forms the new compounds during sintering process. From the BaO–TiO_2 phase diagram, it can be possible that $BaTiO_3$ forms the eutectic liquid phase at around 1322 °C[19] and reacts with Al_2O_3 matrix phase, which resulting in grain growth and inhibiting the densification in the final sintering stage. This phenomenon corresponds to the low relative density of the composites compared to that of the monolithic alumina.

3.2. Crack propagation in unpoled $BaTiO_3/Al_2O_3$ composites

Fig. 4(a) shows cracks propagating from a Vickers indentation in the unpoled 5 mol% $BaTiO_3/Al_2O_3$ composite sintered at 1450 °C. In unpoled composite specimens, domain orientations are random. The cracks

Table 2
Physical properties of the monolithic $A1_2O_3$ and $BaTiO_3/A1_2O_3$ composites in this study

Sintering temp. (°C)	$BaTiO_3$ content (mol%)	Relative density (%)	Hardness (GPa)	Relative X-ray peak intensity of analysed phases to alumina			Mean alumina grain size (μm)
				$BaAl_6TiO_{12}$ (BATO)	$BaAl_{13.2}O_{20.8}$ (BAO)	Total (BATO and BAO)	
1500	0	99.9	17.59±1.06	–	–	–	6.63
1400	3	88.84	9.28±0.23	0.12	0.08	0.20	5.84
	5	84.70	7.26±0.38	0.24	0.11	0.35	3.81
1450	3	89.14	8.49±0.51	0.19	0.03	0.22	6.59
	5	86.12	7.14±0.14	0.39	0.06	0.45	4.17

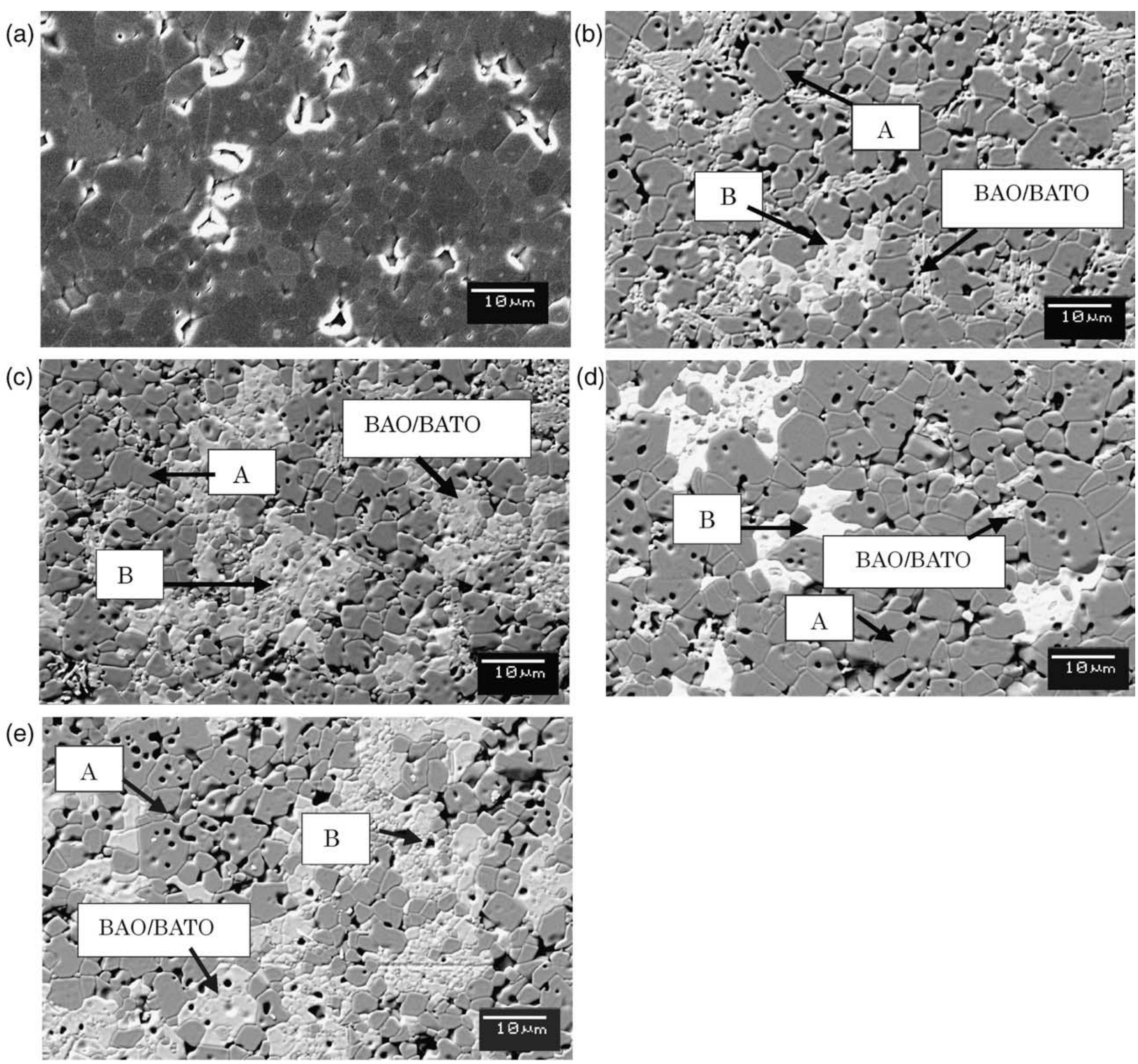

Fig. 3. Scanning electron micrographs of thermal etched surface of $BaTiO_3/Al_2O_3$ composites. (a) Al_2O_3, (b) 3 mol% $BaTiO_3/Al_2O_3$, (c) 5 mol% $BaTiO_3/Al_2O_3$ sintered at 1400 °C, (d) 3 mol% $BaTiO_3/Al_2O_3$, (e) 5 mol% $BaTiO_3/Al_2O_3$ sintered at 1450 °C. Abbreviation: A: Al_2O_3, B: $BaTiO_3$, BAO: $BaAl_{13.2}O_{20.8}$, BATO: $BaAl_6TiO_{12}$.

from the Vickers indentation were equal in length and mutually orthogonal to each other, showing the isotropic crack propagation. The isotropic crack propagation of unpoled PZT has been also reported.[20]

Crack paths in x and y directions for 5 mol% $BaTiO_3/Al_2O_3$ composite sintered at 1450 °C before polarization in higher magnification were shown in Figs. 4(b) and (c), respectively. It is commonly observed that cracks mainly propagated through the aggregates of $BaTiO_3$ and intermediate phases and deflected in the Al_2O_3 matrix grains. It may be result from the much lower elastic modulus of $BaTiO_3$, compared with Al_2O_3. However, it was also observed that the crack arrested at ferroelectric $BaTiO_3$ phase [Fig. 4(c)].

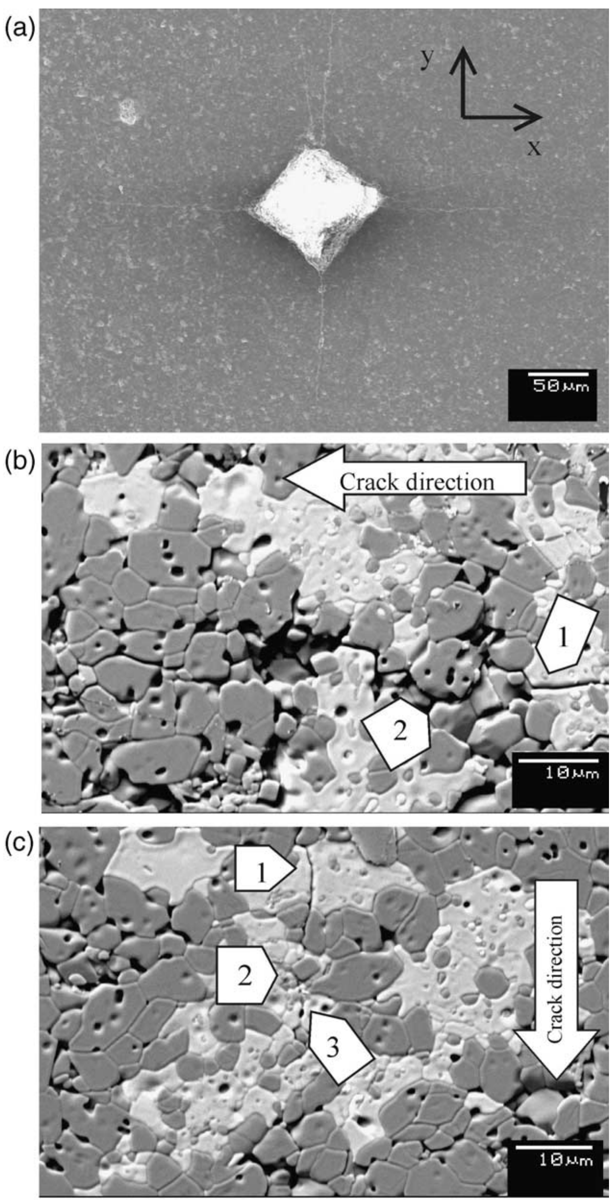

Fig. 4. Cracks propagating from a Vickers indentation in the unpoled 5 mol% $BaTiO_3/Al_2O_3$ composite. Arrows indicate; (1) deflection at or near $BaTiO_3$ particles, (2) crack bridging, (3) crack arresting at or in the intermediate aggregates. (a) Macro view of the indentation crack, (b) crack path in x direction, (c) crack path in y direction.

3.3. *Crack propagation in poled $BaTiO_3/Al_2O_3$ composites*

After poling under 3.75 kV/mm at 120 °C for 10 min, anisotropic crack propagation for 90°-direction indentation was found in $BaTiO_3/Al_2O_3$ composites, as shown in Fig. 5(a). This result is similar to the previous crack propagation study in pure piezoelectric materials.[11,14,15] The length of the crack parallel to the poling direction was shorter than that perpendicular to the poling direction, which might result from anisotropy of fracture toughness. For the 45°-direction indentation [Fig. 5(b)], it was found that all four cracks were almost the same in length.

Figs. 6(a) and (b) show the detailed crack paths perpendicular and parallel to the poling direction, respectively, for poled 5 mol% $BaTiO_3/Al_2O_3$ composites sintered at 1450 °C. It can be observed that the crack perpendicular to the poling direction (x direction) detours and deflects at the $BaTiO_3$ and intermediate aggregates [Fig. 6(a)]. In the other direction (y direction), bridging on the wake crack was found at $BaTiO_3$ grains, as shown in Fig. 6(b).

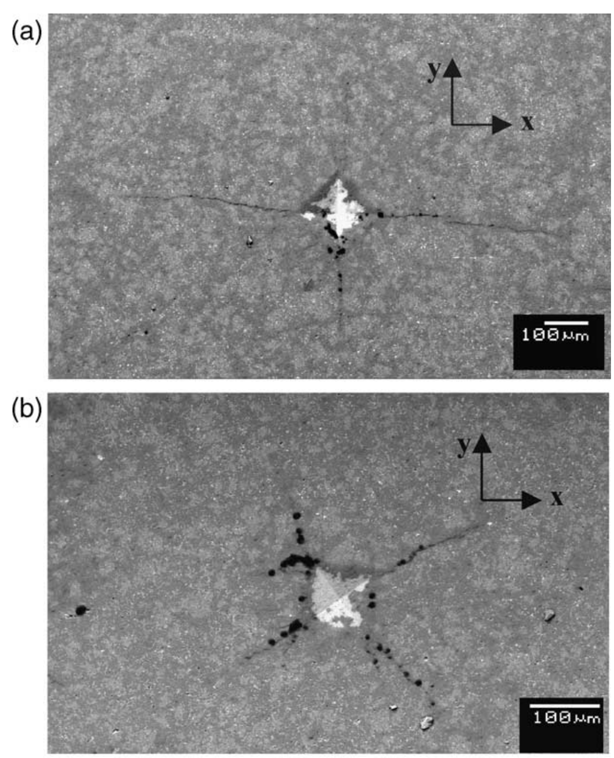

Fig. 5. Macroscopic view of the cracks propagating from Vickers indentation for poled specimens. (a) 90° direction, (b) 45° direction.

3.4. Residual stress after polarization

The residual stresses of unpoled and poled specimens were measured in both of two directions (parallel and perpendicular to the poling directions), which are inversely perpendicular and parallel to the specimen axis, respectively. Figs. 7(a) and (b) show the $\sin^2\varphi$ diagrams for unpoled and poled $BaTiO_3/Al_2O_3$ composites. The relationship between the diffraction angle 2θ and $\sin^2\varphi$ can be approximated by the regression line in the figure.

The X-ray stress measurement of Al_2O_3 was conducted under various applied stresses. Fig. 8 shows the $\sin^2\varphi$ diagram under loading. Thus, the X-ray stress constant (S) of Al_2O_3 sample sintered at 1500 °C is −1250 MPa/°. The residual stresses of monolithic Al_2O_3 and $BaTiO_3/Al_2O_3$ composites in both of two directions are summarized in Table 3.

From Table 3, residual stress of the monolithic Al_2O_3 was non-zero and it can suggest that it was due to surface residual stresses. A compressive residual stress was detected in the unpoled ferroelectric materials.[20] In this study, a compressive residual stress in unpoled $BaTiO_3/Al_2O_3$ composites was also found, where slopes of the curves for both directions parallel and perpendicular to the poling direction were positive. The difference in residual stress of unpoled $BaTiO_3/Al_2O_3$ composites for both directions may be due to the non-uniform of the particle orientation during fabrication process. The residual stress induced in unpoled $BaTiO_3/Al_2O_3$ composites would result from the volume change due to the phase transformation of $BaTiO_3$ from cubic to tetragonal (tensile stress in $BaTiO_3$ particles and compressive stress in Al_2O_3 matrix), associated with the mismatch of

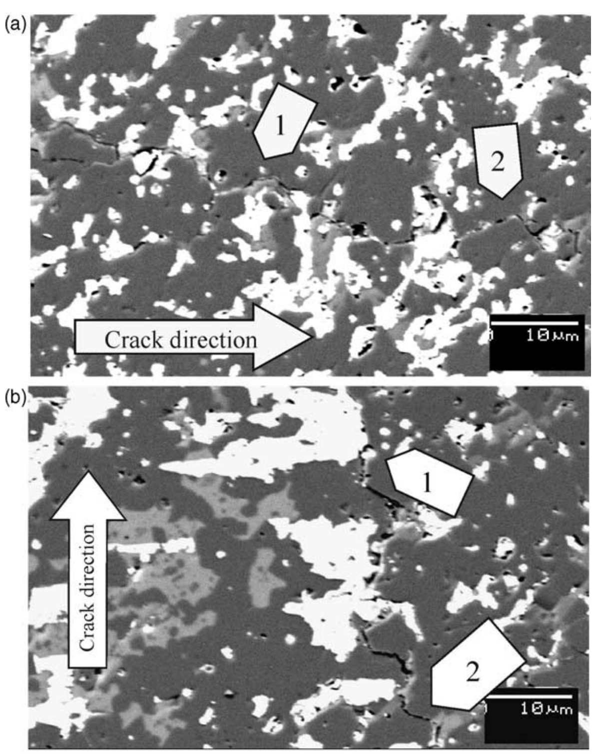

Fig. 6. Crack paths for 5 mol% $BaTiO_3/Al_2O_3$ composite sintered at 1450 °C. Arrows indicate; (1) deflection at or near $BaTiO_3$ particles, (2) crack bridging. (a) x direction (perpendicular to the poling direction), (b) y direction (parallel to the poling direction).

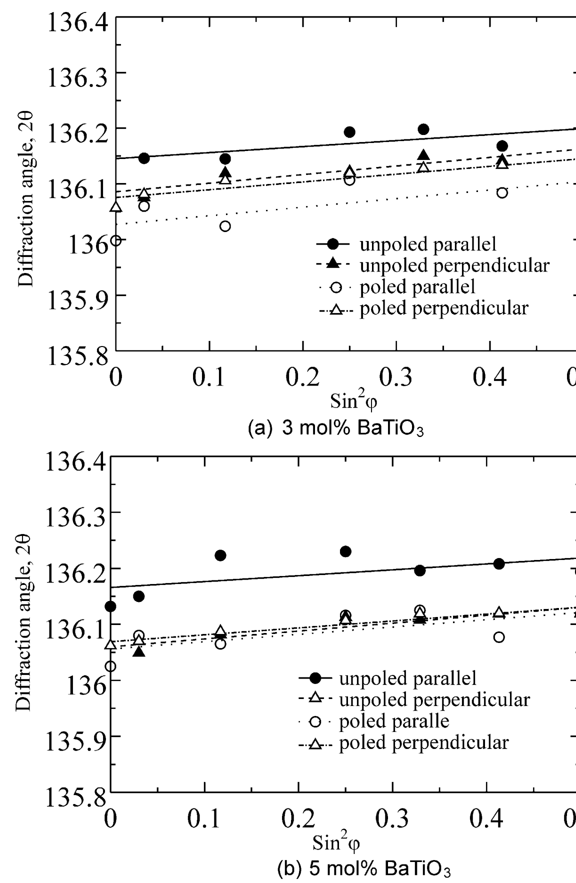

Fig. 7. Relationship between diffraction angle and $\sin^2\varphi$ for (146) diffraction of α-Al_2O_3 matrix for $BaTiO_3/Al_2O_3$ composites sintered at 1450 °C.

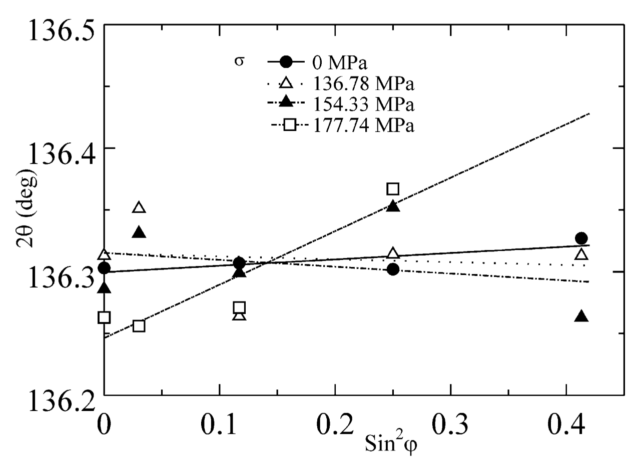

Fig. 8. $Sin^2\varphi$ diagram for Al_2O_3 under loading.

Table 3
Residual stresses for $BaTiO_3/Al_2O_3$ composites

Sintering temp. (°C)	$BaTiO_3$ content (%)	Residual stress (MPa) unpoled		Residual stress (MPa) poled	
		$\sigma_\perp$	$\sigma_\parallel$	$\sigma_\perp$	$\sigma_\parallel$
1500	0	−35.5	−34.2	–	–
1450	3	−191.7	−134.4	−173.6	−187.9
	5	−179.9	−132.1	−154.4	−163.1

thermal expansion of intermediate phases and matrix during cooling process.

After polarization, the residual stresses of $BaTiO_3/Al_2O_3$ composites were still compressive but the residual stress parallel to the poling direction was higher than that perpendicular to the poling direction. From Table 3, the compressive residual stress parallel to the poling direction measured after poling became higher compared with that before poling, while the compressive residual stress perpendicular to the poling direction became lower than that before poling. It is reasonable to consider that the applied electric field would cause a distortion of $BaTiO_3$ accompanied by the generation of internal stress. In the direction perpendicular to the poling direction, structures tend to pull back by the poling field while structures are forced to expand in order to accommodate the longer *c*-axis dimension in the direction parallel to the poling direction, as shown in Fig. 9. The dipoles in the $BaTiO_3$ crystals were possible immediately to align in the poling direction during polarization. Since $BaTiO_3$ structure extended in the poling direction whereas Al_2O_3 matrix should maintain its crystal structure and orientation, the residual stress would be generated in Al_2O_3 matrix. Thus, anisotropic residual stresses were observed in the present composites.

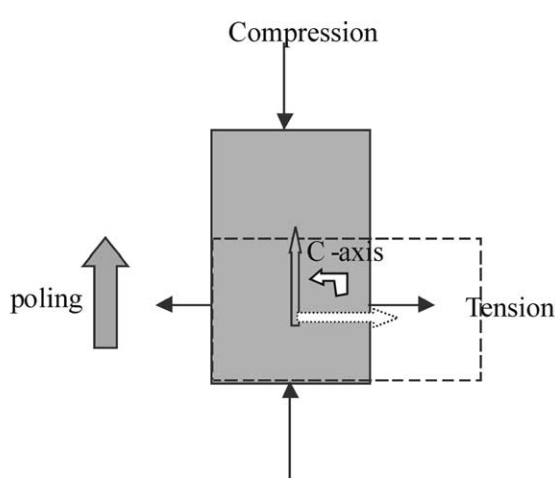

Fig. 9. A schematic of stresses generated from a 90° domain switching under poling electric field.

3.5. Fracture toughness

Fracture toughness of $BaTiO_3/Al_2O_3$ composites before and after polarization was determined by using Indentation Fracture method. Figs. 10(a) and (b) show the relationship between fracture toughness K_{IC} and $BaTiO_3$ content for unpoled and poled $BaTiO_3/Al_2O_3$ composites sintered at 1400 and 1450 °C, respectively. The scatter bands in the figures indicate the 95% confidence interval. Fracture toughness of the $BaTiO_3/Al_2O_3$ composite sintered at 1450 °C was improved with increasing the amount of $BaTiO_3$ addition up to 5 mol% compared to that of the monolithic alumina. Fracture toughness of all poled specimens (90° direction) parallel to the poling direction was improved,

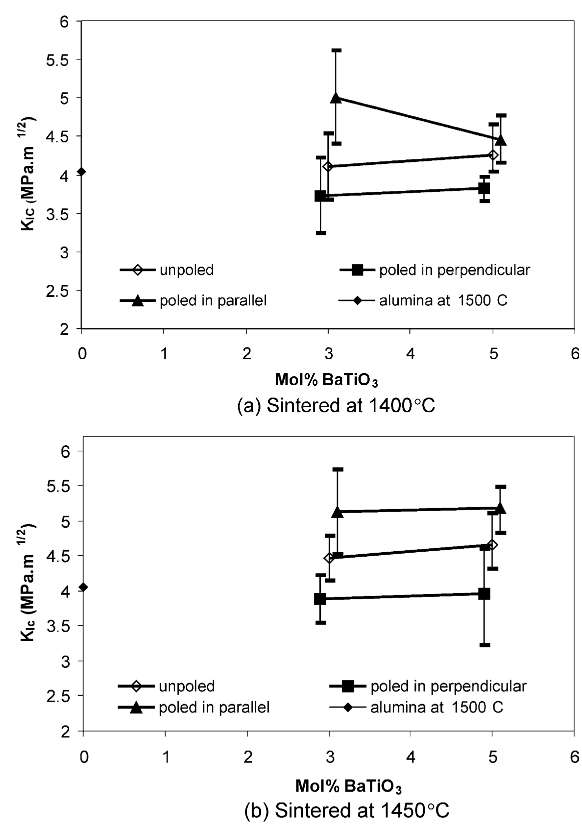

Fig. 10. Relationship between fracture toughness K_{IC} and $BaTiO_3$ content of unpoled and poled $BaTiO_3/Al_2O_3$ composites sintered at (a) 1400 and (b) 1450 °C.

while that perpendicular to the poling direction decreased. Fracture toughnesses for the case of 45° direction indentation were almost the same for two directions, which were not significantly different from those of unpoled specimens. The highest fracture toughness was 5.15 ± 0.61 MPa $m^{1/2}$ in case of the crack parallel to the poling direction for 5 mol% $BaTiO_3/Al_2O_3$ composite sintered at 1450 °C. Although the composite sintered at 1450 °C has a lower $BaTiO_3$ phase content, the material sintered at 1450 °C shows a similar, or even larger, fracture anisotropy than the 1400 °C material. It may be a consequence of the scatter of the indentation data. However, the fracture toughness of a 5 mol% $BaTiO_3/Al_2O_3$ composite sintered at 1400 °C, as shown in Fig. 10(a), decreased due to the low relative density.

The difference in fracture toughness has been explained on the basis of domain switching during crack growth.[15] From X-ray diffraction patterns taken from fracture surfaces of PZT samples in the stable fracture regime, it was found that domain reorientation occurred during fracture where the c axes of many domains became orthogonal to the fracture surfaces. Since a less amount of $BaTiO_3$ piezoelectric remained in the present composites, domain switching could not be clearly detected on fracture surfaces of samples by means of X-ray method. However, it is reasonable to assume that domain switching of the tetragonal structured domains is the main mechanism responsible to the anisotropy of fracture toughness in the preferentially oriented poled composites.

The stress and electric fields around a crack attempt to reorient the domains.[20] The stress distribution near a crack is altered due to constraint of the unswitched material surrounded. 90° Switching occurs under the assistance of high stress near a growing crack tip, which results in toughening, while it depends on the domain orientation. Yang and Zhu[21] reported that stress concentration near a crack tip produced a confined switching zone. The size of the switching zone was large when polarization direction was parallel to the crack, and small when the polarization direction was normal to the crack. The toughness variation induced by domain switching can be evaluated by an approach similar to that widely used in the calculation of transformation toughening of ceramics.[22] The variation of toughness could be determined by the direct calculation of the modified stress intensity factor.[23] The local stress intensity factor at the crack tip, K_{tip}, is given by

$$K_{tip} = K_I + \Delta K \tag{4}$$

where K_I denotes the applied stress intensity factor without toughening mechanism and ΔK denotes the additional stress intensity factor induced by domain switching of $BaTiO_3$ particulars. The fracture toughness of piezoelectric/ferroelectric-particle-dispersed composites can be improved by ΔK. The ΔK depends on the combination of cracking direction and poling direction and consequently the anisotropy of fracture toughness is expected to exhibit in poled composite materials.

4. Conclusions

$BaTiO_3/Al_2O_3$ composites with piezoelectric secondary phase could be produced by a conventional sintering method. The relative density of $BaTiO_3/Al_2O_3$ composites decreased with increasing $BaTiO_3$ content. The microstructure of sintered $BaTiO_3/Al_2O_3$ composites indicated alumina grains with some agglomerated of intermediate phases. However, the fracture toughness of the $BaTiO_3/Al_2O_3$ composites was improved compared to that of the monolithic alumina.

Crack bridging and crack deflection at or near the $BaTiO_3$ phases were increasingly observed in the higher toughness samples, which indicated that the $BaTiO_3$ phase was probably contribute to higher fracture toughness. Although only small amount of $BaTiO_3$ phase remained in the present composites, it obviously contributed to higher fracture toughness parallel to the poling direction after polarization. Crack deflection around $BaTiO_3$ grains was often observed in the poling direction. Anisotropy in residual stress was observed after polarization. It was suggested that the polarization induced the domain reorientation along the poling direction and consequently resulted in the anisotropy in residual stress in the present composites. The anisotropy in crack propagation behavior could not be explained by the residual stress presented in the poled $BaTiO_3/Al_2O_3$ composite, but might be explained by the domain switching mechanism.

Acknowledgements

The authors would like to thank Professor K. Uematsu, Nagaoka University of Technology, for conducting cold isostatic pressing and Tokin Electronic (Japan), Co. Ltd. for advising the polarization technique.

References

1. Noma,T., Wada, S., Sakake, M., Otsuka, T. and Suzuki, T., Indentation fracture of poled barium titanate ceramics. In *Proceedings of the Annual Meeting of the Ceramic Society of Japan*. Yokohama, Japan. The Ceramic Society of Japan, Tokyo, Japan, 1996, pp. 551.
2. Okazaki, K., Mechanical behavior of ferroelectric ceramics. *Ceram. Soc. Bull.*, 1984, **63**(91), 1150–1152.
3. Hwang, H. J., Tajima, Ken-ichi, Sando, M., Toriyama, M. and Niihara, K., Microstructure and mechanical properties of lead zirconate titanate (PZT) nanocomposites with platinum particles. *J. Ceram. Soc. Japan*, 2000, **108**(4), 339–344.

4. Hwang, H. J., Nagai, T., Sando, M., Toriyama, M. and Niihara, K., Fabrication of piezoelectric particle-dispersed ceramic nanocomposite. *J. Eur. Ceram. Soc.*, 1999, **19**, 993–997.
5. Hwang, H. J., Sekino, T., Ota, K. and Niihara, K., Perovskite-type $BaTiO_3$ ceramics containing particulate SiC. *J. Mat. Sci.*, 1996, **31**, 4617–4624.
6. Chen, X. M. and Yang, B., A new approach for toughening of ceramics. *Mat. Lett.*, 1997, **33**, 237–240.
7. Yang, B., Chen, X. M. and Liu, X. Q., Effect of $BaTiO_3$ addition on structures and mechanical properties of 3Y-TZP ceramics. *J. Eur. Ceram. Soc.*, 2000, **20**, 1153–1158.
8. Yang, B. and Chen, X. M., Alumina ceramics toughened by a piezoelectric secondary phase. *J. Eur. Ceram. Soc.*, 2000, **20**, 1687–1690.
9. Chen, X. M., Liu, X. Q., Liu, F. and Zhang, X. B., 3Y-TZP ceramics toughened by $Sr_2Nb_2O_7$ secondary phase. *J. Eur. Ceram. Soc.*, 2001, **21**, 477–481.
10. Seo, S. and Kishimoto, A., Effect of polarization treatment on bending strength of barium titanate/zirconia composite. *J. Eur. Ceram. Soc.*, 2000, **20**, 2427–2431.
11. Schneider, G. A. and Heyer, V., Influence of the electric field on vickers indentation crack growth in $BaTiO_3$. *J. Eur. Ceram. Soc.*, 1999, **19**, 1299–1306.
12. Pohanka, R. C., Freiman, S. W., Okazaki, K. and Toshiro, S.. In *Fracture Mechanics of Ceramics*, ed. R. C. Bradt, A. G. Evans, D. P. H. Hasselman and F. F. Lange. Plenum, New York, 1983, pp. 353–364.
13. Pohanka, R. C., Freiman, S. W. and Rice, R. W., Fracture processes in Ferroic Materials. *Ferroelectrics*, 1980, **28**, 337.
14. Pisarenko, G. G., Chushko, V. M. and Kovalev, S. P., Anisotropy of fracture toughness of piezoelectric ceramics. *J. Am. Ceram. Soc.*, 1985, **68**(5), 259–265.
15. Mehta, K. and Virkar, A. V., Fracture mechanisms in ferroelectric–ferroelastic lead zirconate titanate (Zr:Ti = 0.54:0.46) Ceramics. *J. Am. Ceram. Soc.*, 1990, **73**(3), 567–574.
16. Virker, A. V. and Matsumoto, R. L. K., Ferroelastic domain switching as a toughening mechanism in tetragonal zirconia. *J. Am. Ceram. Soc.*, 1986, **69**(10), C–224-C-246.
17. Niihara, K., Morena, R. and Hasselman, D. P. H., Evaluation of K_{IC} of brittle solids by the indentation method with low crack-to-indent ratios. *J. Mater. Sci. Lett.*, 1982, **1**, 13–16.
18. X-ray Stress Measurement. *The Society of Materials Science*. Yokendo, Japan, 1981.
19. Rase, D.E. and Ray, R., *Eighth Quarterly Progress Report, 1 April–30 June*, The Pennsylvania State University, College of Mineral Industries; Appendix II, 1953, pp. 32.
20. Wang, H. and Singh, R. N., Crack Propagation in piezoelectric ceramics under pure mechanical loading. *Ferroelectrics*, 1998, **207**, 555–575.
21. Yang, W. and Zhu, T., Switch-toughening of ferroelectrics subjected to electric fields. *J. Mech. Phys. Solids.*, 1998, **46**(2), 291–311.
22. McMeeking, R. M. and Evans, A. G., Mechanics of transformation toughening in brittle materials. *J. Am. Ceram. Soc.*, 1982, **65**, 242–246.
23. Reece, M. J. and Guiu, F., Estimation of toughening produced by ferroelectric/ferroelastic domain switching. *J. Eur. Ceram. Soc.*, 2001, **21**, 1433–1436.